Available on CMS information server **CMS CR 1999/013**

CMS Conference Report

6th April 1999

High Precision and Stable Structures for Particle Detectors

S. Da Mota Silva, R. Ribeiro, C. Hauviller

European Laboratory for Particle Physics, CERN - CH 1211 Geneva 23 Switzerland

Abstract

The central detectors used in High Energy Physics Experiments require the use of light and stable structures capable of supporting delicate and precise radiation detection elements. These structures need to be highly stable under environmental conditions where external vibrations, high radiation levels, temperature and humidity gradients should be taken into account. Their main design drivers are high dimension and dynamic stability, high stiffness to mass ratio and large radiation length. For most applications, these constraints lead us to choose Carbon Fiber Reinforced Plastics (CFRP) as structural element. The construction of light and stable structures with CFRP for these applications can be achieved by careful design engineering and further confirmation at the prototyping phase. However, the experimental environment can influence their characteristics and behavior. In this case, the use of adaptive structures could become a solution for this problem. We are studying structures in CFRP with bonded piezoelectric sensors and actuators, able to monitor and compensate the vibrations affecting the performance of these systems. In this paper a detailed description of the simulation model is presented and the results compared with the experimental measurements. The transient response of a plate structure under vibrations with and without feedback control are shown.

Presented at the
SPIE's 6^{th} *Annual International Symposium on Smart Structures and Materials*
Newport Beach, California, 1-5 March 1999

1 Introduction

In the last three decades our understanding of nature's fundamental particles and the forces which act between them has advanced dramatically. The resulting theory, known as Standard Model is one of the greatest intellectual achievements of physics. Even so, we know the Standard Model can only be a stepping-stone to a more complete theory: it leaves too many questions unanswered. How do particles get their masses, for example? And why does nature triplicate the family of basic particles which make up all matter as we know it? At CERN we plan to address these and other fundamental questions of physics with the two general purpose experiments (ATLAS and CMS) that will operate at the Large Hadron Collider (LHC). Both these experiments have the typical onion-like layout of a High Energy Physics (HEP) collider detector with sub-detectors disposed symmetrically around the interaction point. Each of these sub-detectors is able to measure one or more of the parameters that are needed for the full identification of each particle.

Both experiments, CMS and ATLAS, are enormous in size and complexity and cannot be compared with any previous HEP experiment. They are typically a cylinder with 30(45) m long, 15(30) m diameter and weight about 14000(9000) ton, depending on the experiment [1]. The inner part of these detectors is able to measure the passage of charged particles with a precision of tens of μm. These inner sub-detectors are much smaller (6 m length, 4 m diameter and a weight of a few tons) and their support structures must be light, highly stable and stiff in order to achieve these demanding performances [2]. A natural choice of structural materials are CFRP. A particularly interesting point of the conceptual engineering design of these structures is to understand to what extent one is able to measure and control the vibrations of these large CFRP structures.

2 Finite Element Formulation

The equations of motion for a laminated composite plate containing piezoelectric elements can be derived using Hamilton's principle

$$\delta \int_{t_1}^{t_2} (T - U + W_{ext})\, dt = 0 \tag{1}$$

where t_1 and t_2 are arbitrary instants, T is the kinetic energy, U the potential energy (including strain and electrical energies) and W_{ext} the work done by external forces. The term of non conservative work was neglected.

For coupled electro-mechanical systems the kinetic and potential energy terms are defined as

$$T = \int_V \frac{1}{2} \varrho \{\dot{q}\}^T \{\dot{q}\}\, dV \qquad U = \int_V \frac{1}{2} [\, \{S\}^T \{T\} - \{E\}^T \{D\}]\; dV \tag{2}$$

where $\{\dot{q}\}$ is the velocity vector, ϱ the mass density, $\{S\}$ the strain vector, $\{T\}$ the stress vector, $\{E\}$ the electrical field vector, $\{D\}$ the vector of electrical displacements and the integration is done over the volume V of the structure.

2.1 Constitutive Equations

The linear piezoelectric constitutive equations coupling the elastic field and the electric field vector can be expressed by the direct and the converse piezoelectric equations [3]

$$\{D\} = [e]^T \{S\} + [\epsilon^s]\{E\} \tag{3}$$

$$\{T\} = [C^E]\{S\} - [e]\{E\} \tag{4}$$

with $[e]$ the piezoelectric module matrix, $[\epsilon^s]$ the dielectric constants matrix evaluated at constant strain and $[C^E]$ the matrix of the elastic coefficients for the piezoelectric material at constant electric field. Normally one can consider piezoelectric materials as transverse isotrope in the plane normal to the polarization axis ($z - axis$). In the case of piezoceramics (PZT) Equation (3) and Equation (4) can be simplified. Given this isotropy, the coefficients e_{34}, e_{35} and e_{36} are null, and the actuation and/or sensing of torsion movements can not be done. If the material studied is not isotrope transverse in the reference plane the coefficient e_{36} is non zero and can be used to measure or control torsion movements.

In the case of non-isotropic materials and when the piezoelectric is cut in other directions different from its orthotropy axes, the stress and strain relations in the material coordinate system are related to the global coordinate system by the following expressions

$$\{T\}_m = [R]\{T\}_g \qquad\qquad \{S\}_m = [R]^{-T}\{S\}_g \tag{5}$$

where m stands for material coordinates and g for global coordinates. $[R]$ is the transformation matrix between the two coordinate systems.

2.2 Strain-Displacements Relations

Under the same assumptions and restrictions as in the classical laminate theory, the displacement field of the first-order shear deformation theory is of the form [4]

$$\begin{aligned} u(x,y,z,t) =& u_0(x,y,t) + z\phi_x(x,y,t) \\ v(x,y,z,t) =& v_0(x,y,t) + z\phi_y(x,y,t) \\ w(x,y,z,t) =& w_0(x,y,t) \end{aligned} \tag{6}$$

where u_0, v_0 and w_0 are the in-plane and transverse displacements of a point (x, y) in the mid-plane, and ϕ_x and ϕ_y are the rotations of a transverse normal about the y and x axes. Substituting Equation (6) into the infinitesimal strain relations we obtain $\{S\} = \{S^0\} + z\{\kappa\}$ where $\{S^0\} = \{S_x^0, S_y^0, 0, \gamma_{yz}^0, \gamma_{xz}^0, \gamma_{xy}^0\}^T$ are the membrane strains and $\{\kappa\} = \{\kappa_x, \kappa_y, 0, 0, 0, \kappa_{xy}\}^T$ are the bending strains. This equation can be rewritten as

$$\begin{bmatrix} S_x \\ S_y \\ S_z \\ \gamma_{yz} \\ \gamma_{xz} \\ \gamma_{xy} \end{bmatrix} = \begin{bmatrix} \frac{\partial u_0}{\partial x} \\ \frac{\partial v_0}{\partial y} \\ 0 \\ \frac{\partial w_0}{\partial y} + \phi_y \\ \frac{\partial w_0}{\partial x} + \phi_x \\ \frac{\partial u_0}{\partial y} + \frac{\partial v_0}{\partial x} \end{bmatrix} + z \begin{bmatrix} \frac{\partial \phi_x}{\partial x} \\ \frac{\partial \phi_y}{\partial y} \\ 0 \\ 0 \\ 0 \\ \frac{\partial \phi_x}{\partial y} + \frac{\partial \phi_y}{\partial x} \end{bmatrix} \tag{7}$$

The generalized strain vector, $\{\bar{S}\} = \{S_x^0, S_y^0, \gamma_{xy}^0, \kappa_x, \kappa_y, \kappa_{xy}, \gamma_{xz}^0, \gamma_{yz}^0\}^T$, can be defined in terms of the nodal displacements vector $\{q\}$ and in terms of the differential operator matrix $[L]$ by $\{\bar{S}\} = [L]\{q\}$. Expanding all the terms one obtains

$$\begin{bmatrix} S_x^0 \\ S_y^0 \\ \gamma_{xy}^0 \\ \kappa_x \\ \kappa_y \\ \kappa_{xy} \\ \gamma_{xz}^0 \\ \gamma_{yz}^0 \end{bmatrix} = \begin{bmatrix} \frac{\partial}{\partial x} & 0 & 0 & 0 & 0 \\ 0 & \frac{\partial}{\partial y} & 0 & 0 & 0 \\ \frac{\partial}{\partial y} & \frac{\partial}{\partial x} & 0 & 0 & 0 \\ 0 & 0 & 0 & z\frac{\partial}{\partial x} & 0 \\ 0 & 0 & 0 & 0 & z\frac{\partial}{\partial y} \\ 0 & 0 & 0 & z\frac{\partial}{\partial y} & z\frac{\partial}{\partial x} \\ 0 & 0 & \frac{\partial}{\partial x} & 1 & 0 \\ 0 & 0 & \frac{\partial}{\partial y} & 0 & 1 \end{bmatrix} \begin{bmatrix} u_0 \\ v_0 \\ w_0 \\ \phi_x \\ \phi_y \end{bmatrix} \tag{8}$$

2.3 Stress-Strain Relations

The stress and moment resultant vector is defined by

$$\begin{aligned} &\{\bar{N}\} = \{N_x, N_y, N_{xy}, M_x, M_y, M_{xy}, Q_x, Q_y\}^T \\ &\{N_x, N_y, N_{xy}, Q_x, Q_y\} = \sum_{k=1}^{N} \int_{-h/2}^{h/2} (T_x, T_y, T_{xy}, T_{xz}, T_{yz})\, dz \qquad \{M_x, M_y, M_{xy}\} = \sum_{k=1}^{N} \int_{-h/2}^{h/2} (T_x, T_y, T_{xy}) z\, dz \end{aligned} \tag{9}$$

and can be written, taking into account Equation (4), as the result of two components

$$\{\bar{N}\} = [\bar{D}]\{\bar{S}\} - \{X_p\} \tag{10}$$

One, $[\bar{D}]\{\bar{S}\}$, represents the resultant of the mechanical stresses and the other, $\{X_p\}$, the equivalent stress created by the piezoelectrics as a consequence of the actuation strains. The matrix $[\bar{D}]$ is the transformed stiffness matrix of the plate in the plate axis system, and is defined in terms of the extensional stiffnesses, the bending stiffnesses and the bending-extensional coupling stiffnesses. The piezoelectric resultant for the laminate is defined by

$$\{X_p\} = \begin{bmatrix} \{E^N\} \\ \{E^M\} \\ 0 \end{bmatrix} = \begin{bmatrix} \sum_{k=1}^{N} \int_{z_{k-1}}^{z_k} \bar{[e]}^{(k)} \{E\}^{(k)} \, dz \\ \sum_{k=1}^{N} \int_{z_{k-1}}^{z_k} \bar{[e]}^{(k)} \{E\}^{(k)} z \, dz \\ 0 \end{bmatrix} = \begin{bmatrix} \sum_{k=1}^{N} \bar{[e]}^{(k)} V^{(k)} \\ \sum_{k=1}^{N} \bar{[e]}^{(k)} V^{(k)} z_k^0 \\ 0 \end{bmatrix} \tag{11}$$

where $\{E\}^{(k)} = V^{(k)}/h_k$. $V^{(k)}$ is the electric voltage applied across the K^{th} layer, h_k is the thickness of the K^{th} layer, and z_k^0 is the z distance of the lamina mid-plane from the laminate mid-plane, defined by $z_k^0 = \frac{1}{2}(z_k + z_{k-1})$ [5].

2.4 Finite Element Discretization

The displacement and the electrical potential can be defined in terms of i nodal variables via the shape functions matrices $[N_q]$ and $[N_\phi]$

$$\{q\} = [N_q]\{q_i\} \qquad \{\phi\} = [N_\phi]\{\phi_i\} \tag{12}$$

where $\{q_i\}$ is the mechanical generalized coordinates and $\{\phi_i\}$ the electrical generalized coordinates. Writing the electric field and Equation (8) in terms of nodal variables one obtains for the finite element discretization the following set of expressions

$$\begin{aligned} \{S\} = [L]\{q\} = [B_q]\{q_i\} \qquad [B_q] = [L][N_q] \\ \{E\} = -\nabla\{\phi\} = [B_\phi]\{\phi_i\} \qquad [B_\phi] = -\nabla[N_\phi] \end{aligned} \tag{13}$$

2.5 Equations of motion

Considering only discrete applied external forces, W_{ext} can be written as

$$W_{ext} = \sum_{i=1}^{nf} \{q\}^T \{F_c\} \tag{14}$$

where $\{F_c\}$ is the external force vector acting at x_i and nf is the number of applied external forces. The equations of motion of the electro-mechanical system can be obtained by solving Equation (1).

$$\int_{t_1}^{t_2} \{ \int_V (\varrho \{\dot{\delta q}\}^T \{\dot{q}\} - \{\delta S\}^T [C^E]\{S\} + \{\delta E\}^T [\epsilon^s]\{E\} + \{\delta E\}^T [e]^T \{S\} + \{\delta S\}^T [e]\{E\}) \, dV + \sum_{i=1}^{nf} \{\delta q\}^T \{F_c\} \} \, dt = 0 \tag{15}$$

The first term in Equation (15) can be integrated by parts and Equation (12) substituted in. Allowing arbitrary variations of $\{q\}$ and $\{\phi\}$, two matrix equations in the generalized coordinates are obtained

$$[M_{mm}]\{\ddot{q}\} + [K_{mm}]\{q\} - [K_{em}]\{\phi\} = F \tag{16}$$

$$[K_{em}]^T \{q\} + [K_{ee}]\{\phi\} = 0 \tag{17}$$

where the mass and the mechanical stiffness matrix are defined as

$$[M_{mm}] = \int_V \varrho [N_q]^T [N_q]\, dV \qquad [K_{mm}] = \int_V [B_q]^T [C^E] [B_q]\, dV \tag{18}$$

the coupled electrical/mechanical stiffness and the piezoelectric stiffness matrix as

$$[K_{em}] = \int_V [B_q]^T [e] [B_\phi]\, dV \qquad [K_{ee}] = \int_V [B_\phi]^T [\epsilon^s] [B_\phi]\, dV \tag{19}$$

and the forcing matrix as

$$\{F\} = \sum_{i=1}^{nf} [N_q]^T \{F_c\} \tag{20}$$

Equations (16) and (17) represent, respectively, the actuator and the sensor equations used in the simulation models.

3 Experimental set-up

The experimental set-up (Fig. 1) comprises a graphite T300/epoxy cantilever beam with two symmetrically bonded piezoceramics. The piezoelectric patches are sampled and controlled by a 12-bit Data Acquisition Board with a maximum sampling rate of 500 KHz.

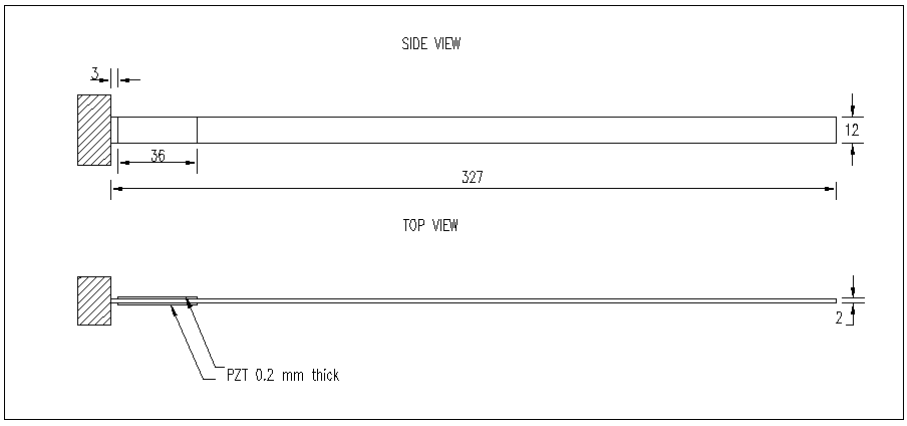

Figure 1: The experimental set-up. One pair of PZT patches attached to a carbon fiber cantilever beam [mm].

The beam, with a stacking sequence of $[0/45^\circ]_{2s}$, has an Young's Modulus of 53.6 GPa and density of 1438 Kg/m^3. The piezoceramic pair is a 0.2 mm thick P1-91 piezoceramic block with 36 mm long and 12 mm wide, polarized in the same direction. Its electro-mechanical properties are listed in Table 1.

The piezoceramics are bonded near the clamped edge of the beam in order to maximize the bending moment. In the simulations it was assumed that the thin bonding layer between the piezoelectric and the composite beam can be neglected [6].

4 Simulation and Experimental Results for Static Loads

Static sensing and actuation mechanisms were investigated for a carbon/epoxy plate described before. Analytical models are based in plate and solid brick formulations. Voltage is considered as an additional degree of freedom. The experimental relation between the applied voltage in the actuator and the displacement at different lengths of the beam (Fig. 2) was used for comparison with the simulations.

The simulated points of Fig. 3 were obtained when a constant voltage of 10 Volt is applied on both piezoceramics. As expected [7] one can find a good agreement between plate and solid brick element formulations. The good

Table 1: Material properties for the P1-91 piezoceramic material.

$C_{11}^E\ [N/m^2]$	12.09x10^{10}	$d_{31}\ [m/V]$	-247x10^{-12}
$C_{12}^E\ [N/m^2]$	7.63x10^{10}	$d_{33}\ [m/V]$	600x10^{-12}
$C_{13}^E\ [N/m^2]$	7.31x10^{10}	$d_{15}\ [m/V]$	509x10^{-12}
$C_{33}^E\ [N/m^2]$	11.26x10^{10}	$\epsilon_{11}^s/\epsilon_0$	1820
$C_{44}^E\ [N/m^2]$	3.36x10^{10}	$\epsilon_{33}^s/\epsilon_0$	1461
$C_{66}^E\ [N/m^2]$	2.23x10^{10}	$\varrho\ [Kg/m^3]$	7410

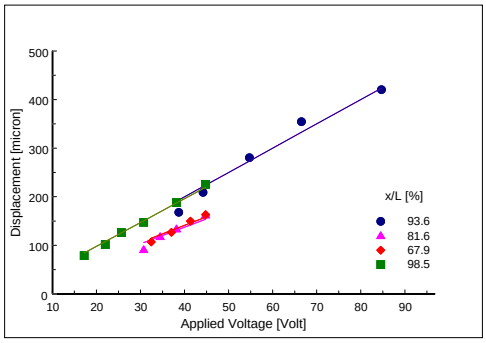

Figure 2: Experimental relation between the applied voltage and the displacement at different lengths of the beam.

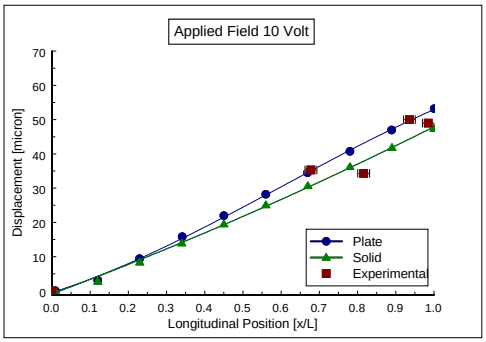

Figure 3: Actuation Mechanism: static deflection shape for an applied voltage of 10 Volt. The experimental points were obtained from Fig. 2.

agreement between the model and the experimental results attests for the validity of the model. Sensing mechanism was evaluated by applying a constant tip load. Output sensor voltages were then determined and are presented in Fig 4.

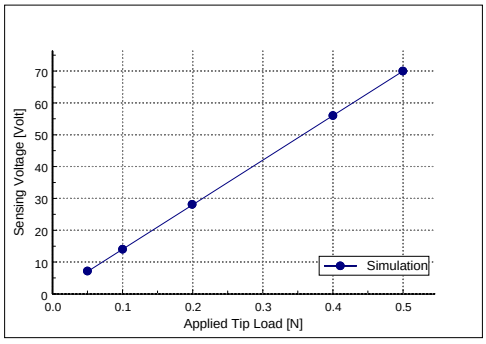

Figure 4: Sensing Mechanism: sensing voltages for several tip loads.

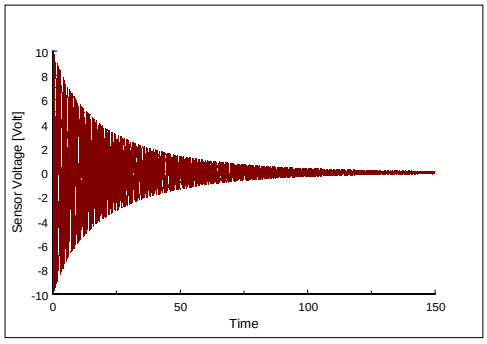

Figure 5: System transient response.

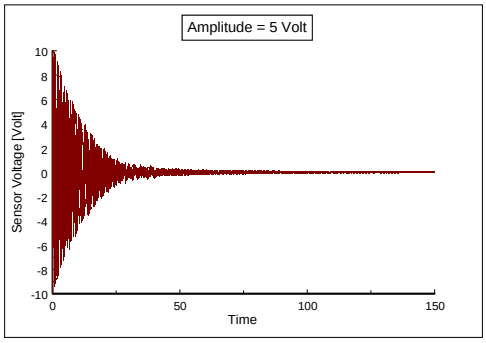

Figure 6: Effect of constant amplitude feedback (5 Volt) on the transient response of the system.

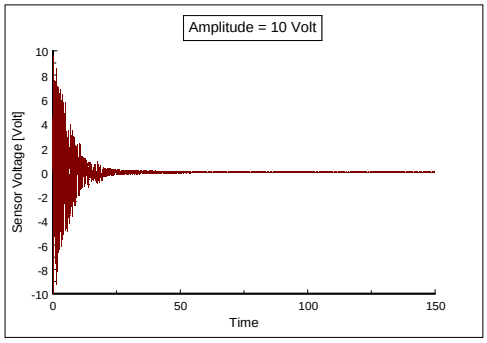

Figure 7: Effect of constant amplitude feedback (10 Volt) on the transient response of the system.

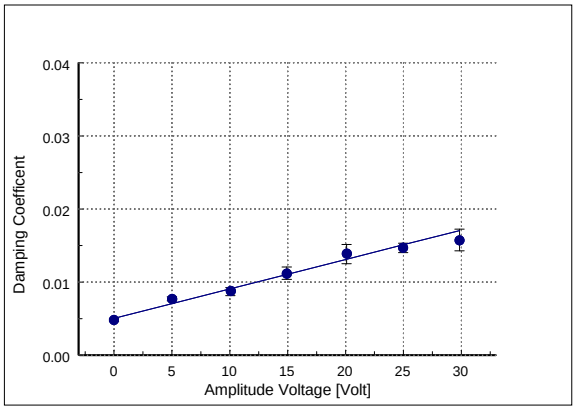

Figure 8: Effect of constant amplitude feedback on the damping coefficient of the system.

5 Vibration Control

To study the dynamic problem of vibration control we will consider that one piezoelectric acts as a sensor and the other one as an actuator. For the control of the vibrations we will consider constant amplitude and constant gain feedback control.

5.1 Constant amplitude feedback control

In this case the feedback amplitude is constant and opposite to the sensing voltage. The system transient response is presented in Fig. 5 and the effect of control feedback on Fig. 6 and Fig. 7.

The piezoelectric mechanical/electrical coupling characteristic can be used to increase the damping of the system. The damping coefficient of the system is calculated by means of the logarithmic decrement, δ. For small damping ratios ($\zeta \ll 1$) the expression can be defined by Equation (21), where n is the number of cycles.

$$\zeta = \frac{\delta}{2\pi} = \frac{1}{2\pi n} \log \frac{x_i}{x_{i+n}} \tag{21}$$

As expected, for small oscillations, the damping coefficient increases linearly with the constant applied voltage (Fig. 8): $\zeta = 0.005 + 0.0004V$.

5.2 Constant gain feedback control

The sensor voltage, V^s, is fed back to the actuator multiplied by a feedback gain G according to Equation (22). The gain, constant in time, is changed in order to evaluate its control effectiveness.

$$V^a = GV^s \tag{22}$$

The bending moment applied by the actuator to the beam is directly proportional to the input voltage applied to the piezoceramic. Its upper limit is given by the voltage limitations of our experimental set-up. Fig. 9 and Fig. 10 present the transient response of the system for different gains.

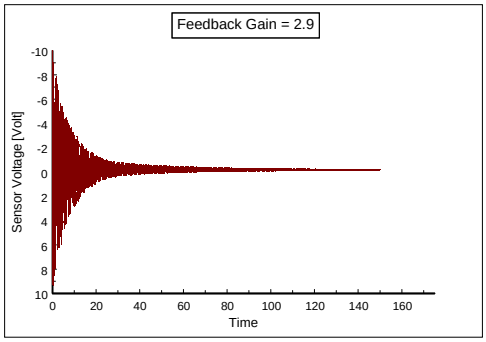

Figure 9: Effect of constant gain feedback (2.9) on the transient response of the system.

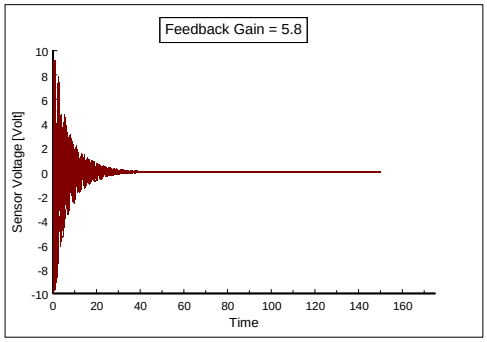

Figure 10: Effect of constant gain feedback (5.8) on the transient response of the system.

The damping coefficient of the system as a function of the feedback gain is presented in Fig. 11, $\zeta = 0.005 + 0.00014G$.

5.3 Frequency analysis

The first mode of vibration was obtained as well as the corresponding modal shape (flexural mode). The comparison between finite element method predictions and experimental measurements is summarized in Table 2.

A maximum deviation of 2.1% is found when the experimental result is compared with the finite element results. The experimental first mode power spectral density for open and close loop (amplitude control voltage equal to 5 Volt) is presented in Fig. 12 and Fig. 13.

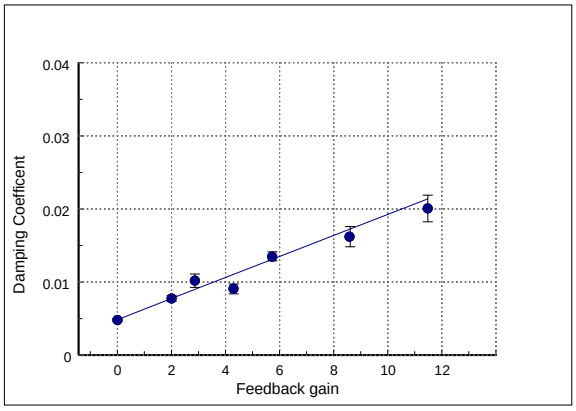

Figure 11: Effect of constant gain feedback on the damping coefficient of the system.

Table 2: First natural frequency obtained by simulation and measurement [Hz].

	Frequency [Hz]	Error [%]
EXPERIMENTAL	21.12	-
FEM - PLATE	20.67	2.13
FEM - SOLID	20.86	1.23

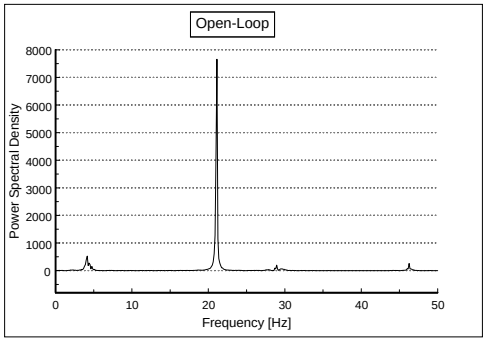

Figure 12: Experimental first mode power spectral density for open loop system.

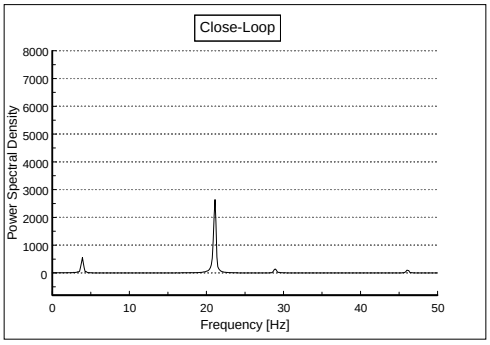

Figure 13: Experimental first mode power spectral density for close loop system - amplitude control voltage equal to 5 Volt.

We can observe a first natural frequency around 21 Hertz. The peak around 5 Hertz is a parasite frequency which was not identified. We can verify that feedback control leads to a lower power spectral density when compared to the open loop system.

6 Conclusions

We show in this paper that the mathematical models and the assumptions used for the simulation of a composite beam with piezoceramic patches, are accurate in the prediction of its static and dynamic behavior. A good agreement was found for the deflection shape of the beam when a constant voltage is applied to the piezoceramics and in the prediction of the first natural frequency. The effectiveness of *constant gain* and *constant amplitude* feedback control was experimentally evaluated by the comparison of the corresponding variation of the damping coefficient. These simple feedback control mechanisms already allow an efficient damp of the first mode of our system. A more elaborated control technique will certainly be needed for the case of more complex structures subjected to external excitations. In High Energy Particle detectors the requirements of high dimensional stability, high stiffness to mass ratio and maximum displacements are of the order of tens of microns. These requirements orient the design of their support structures towards the use of the composite sandwich technology. Also, the wide range of possible combination of core and facing materials provides a higher versatility on the final mechanical properties of these structures. The finite element models used for this work will be modified for sandwich structures and adjusted by similar experimental measurements.

Acknowledgments

One of us, S. Da Mota Silva, would like to thank the financial support by Fundação para a Ciência e a Tecnologia, Lisboa, Portugal in the framework of a cooperation program between Agência de Inovação, Lisboa, Portugal and the European Laboratory for Particle Physics, Geneva, Switzerland. The authors would like to thank to their colleagues Kurt Artoos, J. C. da Silva and W. Coosemans, and to the CERN/TA1 team for their support on the experimental setup.

References

[1] *The CMS Tracker Project - Technical Design Report*, CERN/LHCC 98-6, 1998.

[2] C. Hauviller, "High Performance Composite Structures for High Precision Particle Detectors", in *11th International Conference on Composite Materials*, Gold Coast, Australia, July 1997.

[3] H.S. Tzou and C.I. Tseng, "Distributed piezoelectric sensor/actuator design for dynamic measurement/control of distributed parameter systems: a piezoelectric finite element approach", *Journal of Sound and Vibration*, 138(1), pp 17-34, 1990.

[4] J.N. Reddy, *Mechanics of laminated composite plates - Theory and analysis*, CRC Press, 1997

[5] K. Chandrashekhara and A. N. Agarwal, "Active vibration control of laminated composite plates using piezoelectric devices: a finite element approach", *Journal of Intelligent Materials and Structures*, Vol.4, pp. 496-508, October 1993.

[6] E.F. Crawley and J. Luis, "Use of piezoelectric actuators as elements of intelligent structures", *AIAA Journal*, 25(10), pp. 1373-1385, 1987.

[7] A. Suleman and V.B. Venkayya, "A simple finite element formulation for a laminated composite plate with piezoelectric layers", *Journal of Intelligent Materials and Structures*, Vol.6, pp. 776-782, November 1995.